Deep Learning Based Lungs Disease Classification Using Chest X-ray Image Dataset

Nalankilli R [1], Sriram K [2], Kukku Youseff [3], Kalyani Desikan [4]

[1,2,3,4] School of Advanced Science, VIT Chennai

E-mail address: [1]nalankilli.r2022@vitstudent.ac.in , [2]sriram.k2022@vitstudent.ac.in

[3]kukku.youseff2022@vitstudent.ac.in , [4]kalyanidesikan@vit.ac.in

Abstract

Chest X-RAY images (CXR) facilitate the prompt and convenient detection of lung diseases. This paper presents a detailed account of the construction and implementation of deep learning models for disease classification based on the National Institutes of Health (NIH) chest X-ray dataset. The models, developed using a convolutional neural network (CNN), are trained on a comprehensive dataset comprising 112,120 X-ray images with corresponding disease labels, collected from a total of 30,805 individual patients. The process of building the model involves several crucial stages. Firstly, the NIH chest X-ray dataset is obtained from the official NIH website, providing a wealth of diverse X-ray images for depicting healthy individuals and patients with lung diseases. Subsequently, data pre-processing techniques are applied, including resizing the images to a standardized dimension and normalizing the pixel values to ensure consistent and reliable inputs. Our proposed approach is a single-step, comprehensive learning method in which raw CXR images are fed directly into a deep learning model. This model effectively captures and extracts significant features from the images, enabling accurate identification of different disease categories. To evaluate the performance of the model, validation metrics used is ROC curve analysis. These metrics provide a comprehensive assessment of the model's classification capabilities, ensuring its reliability and effectiveness.

KEYWORDS: Deep learning, Classification, Chest X-ray, Disease detection, Medical imaging.

1. Introduction

Chest X-rays play a crucial role in the diagnosis and evaluation of thoracic pathologies, providing valuable insights into various lung and heart conditions. The availability of large-scale annotated datasets, such as the NIH Chest X-ray dataset, has revolutionized research and development in the field of medical imaging analysis. This dataset, consisting of over 100,000 chest X-ray images, annotated with different thoracic pathologies, offers a rich resource for studying and understanding a wide range of pulmonary and cardiac diseases. In this paper, we aim to explore and analyse the thoracic pathologies present in the NIH Chest X-ray dataset. By leveraging advanced machine learning and deep learning techniques, we seek to develop models capable of accurately identifying and classifying these pathologies. Through this analysis, we hope to contribute to the field of medical imaging by improving the accuracy and efficiency of thoracic pathology diagnosis, aiding radiologists and healthcare professionals in their decision-making process. The dataset encompasses a diverse array of thoracic abnormalities, including but not limited to atelectasis, cardiomegaly, effusion, infiltration, mass, nodule, pneumonia, pneumothorax, consolidation, edema, emphysema, fibrosis, pleural thickening, and hernia. Each pathology presents unique challenges and requires careful analysis and interpretation of chest X-ray images. By examining this dataset, we aim to gain insights into the distribution, prevalence, and characteristics of these thoracic pathologies.

Additionally, we seek to evaluate the performance of state-of-the-art machine learning models in accurately detecting and classifying these abnormalities. Understanding the

strengths and limitations of these models will enable us to identify areas for improvement and further enhance their clinical utility. Through our research, we hope to contribute to the growing body of knowledge in medical imaging analysis and provide valuable insights into the accurate detection and classification of thoracic pathologies. This paper will provide a comprehensive analysis of the NIH Chest X-ray dataset, showcasing the potential for advanced machine learning techniques to improve diagnostic accuracy and assist healthcare professionals in delivering efficient and effective patient care.

1.1Thoratic disease of NIH data set

Upon analaysis we found these 14 disease are the most privalining diseases among the data set

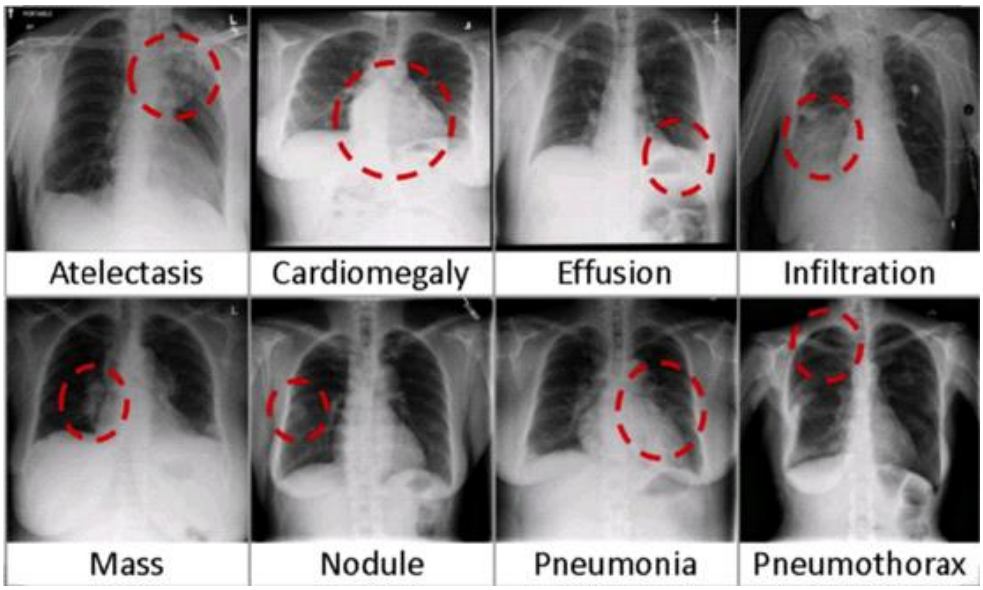

Fig 1: A sample of the disease label from the dataset

1.1.1Atelectasis

It occurs when one or more areas of the lung collapse or do not fully expand. It can be caused by blockage of the airways (obstructive atelectasis), compression of the lung tissue (compressive atelectasis), or inadequate production of surfactant (non-obstructive atelectasis). Common causes include mucus plugs, tumors, foreign objects, or weakened lung tissue.

1.1.2. Cardiomegaly:

Cardiomegaly refers to an enlarged heart, which can be a sign of an underlying heart condition. It is often associated with conditions such as heart failure, coronary artery disease, high blood pressure (hypertension), heart valve abnormalities, or congenital heart defects. Cardiomegaly can strain the heart and affect its ability to pump blood efficiently.

1.1.3. Effusion:

Pleural effusion occurs when excess fluid accumulates in the pleural space, the space between the lungs and the chest wall. It can be caused by various factors, including infections (such as pneumonia or tuberculosis), congestive heart failure, liver disease, kidney disease, malignancies, or inflammation. Symptoms may include chest pain, shortness of breath, and cough.

1.1.4. Infiltration:

Infiltration refers to the presence of abnormal substances in the lung tissue, such as fluid, cells, or inflammatory exudates. It can result from infections (e.g., pneumonia, tuberculosis), inflammatory lung diseases (e.g., sarcoidosis), aspiration of foreign material, drug reactions, or malignancies. Infiltrates may appear as patchy or diffuse opacities on a chest X-ray.

1.1.5. Mass:

A lung mass refers to an abnormal growth or tumor in the lung or surrounding tissues. It can be benign (non-cancerous) or malignant (cancerous). Lung masses can be caused by various factors, including lung cancer, metastatic cancer from other organs, benign tumors (e.g., hamartoma), or granulomas. Further evaluation, such as biopsy or imaging, is needed to determine the nature of the mass.

1.1.6. Nodule:

A lung nodule is a small, round or oval-shaped lesion in the lung, typically measuring less than 3 centimeters in diameter. Nodules can have various causes, including infections (e.g., fungal infections), benign tumors (e.g., granulomas, hamartomas), or malignant lung cancer. Further evaluation, such as follow-up imaging or biopsy, is often required to determine the nature of the nodule.

1.1.7. Pneumonia*:* Pneumonia is an infection that causes inflammation and consolidation of the lung tissue. It can be caused by bacteria, viruses, fungi, or other microorganisms. Common symptoms include cough, fever, chest pain, and difficulty breathing. Chest X-rays can show areas of opacity or consolidation in the lungs, indicating the presence of infection.

1.1.8. Pneumothorax**:** Pneumothorax occurs when air enters the pleural space, causing the lung to collapse. It can be spontaneous (without an obvious cause), traumatic (due to injury or medical procedures), or associated with underlying lung diseases (e.g., emphysema). Symptoms include sudden chest pain, shortness of breath, and decreased breath sounds on examination. Chest X-rays may show a collapsed lung or the presence of air in the pleural space.

1.1.9 Emphysema*:* Emphysema is a lung condition characterized by the destruction of air sacs in the lungs, leading to difficulty in breathing. It is commonly associated with smoking and chronic obstructive pulmonary disease (COPD).

1.1.10 Hernia*:* Hernia refers to the protrusion of an organ or tissue through an abnormal opening in the body's muscular wall. In the context of the dataset, it may refer to abnormalities in the diaphragm or other structures.

1.1.11 Pleural Thickening**:** Pleural thickening occurs when the membranes (pleura) surrounding the lungs become thickened and stiff. It is often a result of lung infections, asbestos exposure, or other lung diseases.

1.1.12 Fibrosis: Pulmonary fibrosis is a condition characterized by the scarring and thickening of lung tissues. It can be caused by various factors, including exposure to environmental toxins, autoimmune diseases, or idiopathic reasons.

***1.1.13 Edema*:** Edema refers to the accumulation of excess fluid in the body's tissues. Pulmonary edema specifically refers to fluid buildup in the lungs, which can result from heart problems, lung infections, or other medical conditions.

1.1.14 Consolidation: Consolidation in the context of lung imaging refers to regions where the lung tissue becomes denser due to the filling of air spaces with fluid, blood, or other substances. It is often a sign of pneumonia or other respiratory infections.

1.2. Literature review

Previous works in classification model evaluation have extensively studied accuracy, precision, F-score, specificity, and sensitivity. These metrics have been used to assess model performance in various domains, including medical diagnostics and fraud detection. Accuracy measures overall correctness, precision focuses on true positives, F-score balances precision and recall, specificity evaluates true negative rate, and sensitivity assesses true positive rate. These metrics have been instrumental in evaluating classification models' effectiveness and have been subject to ongoing research for further refinement and application.

Souid et al.,[1] a deep learning model based on the MobileNet V2 architecture is proposed for the classification of lung diseases from chest X-rays. The authors evaluate their model using a dataset of 10,000 chest X-rays and report an accuracy of 94%. This research suggests that deep learning techniques can be utilized to develop accurate and reliable systems for the automatic classification of lung diseases from chest X-rays.

Zaidi et al.[2] presented a deep learning-based approach for TB classification using the NIH CXR dataset. They applied various deep learning algorithms, achieving high accuracy with decision tree and ADA boost algorithms. The study demonstrated the potential of deep learning techniques and emphasized the effectiveness of ensemble methods. However, more details about the algorithms used would have enhanced the understanding of the experimental setup.

Tang et al.[3] proposes a generative adversarial one-class classifier for identifying abnormal chest X-ray images. The authors aim to improve the accuracy of abnormality detection in medical imaging. The results demonstrate the effectiveness of their approach in accurately classifying abnormal chest X-ray images, showcasing its potential for clinical applications.

Elshennawy and Ibrahim[4] presents a deep learning-based framework for the detection of pneumonia using chest X-ray images. The authors aim to leverage the power of deep learning models to accurately identify pneumonia cases. The paper, however, does not provide specific details regarding the deep learning algorithms used. The study highlights the potential of deep learning techniques for pneumonia detection from chest X-ray images

Abdullahi et al.[5] present a study on the application of deep learning for pneumonia classification. The authors aim to utilize deep learning algorithms to accurately identify pneumonia cases from chest X-ray images during the COVID-19 pandemic. The study highlights the potential of deep learning techniques in improving the accuracy of pneumonia diagnosis. However, specific details regarding the deep learning algorithms used and their performance metrics are not provided.

Jaiswal et al.[6] propose a deep learning approach for identifying pneumonia in chest X-rays. They leverage the power of deep learning algorithms to accurately classify pneumonia cases.

The authors emphasize the potential of their approach in improving the diagnosis of pneumonia from X-ray images. However, further details about the specific deep learning techniques used in the study are not provided.

Yuanyuan Li et al.[7] evaluated the accuracy of deep learning in automated pneumonia detection using chest X-ray images. They synthesized the findings from various studies in the field. The authors aimed to assess the overall performance of deep learning models for pneumonia detection. The review provides insights into the potential of deep learning algorithms for accurate and automated pneumonia identification from chest X-ray images.

2. Methodology

The project focuses on utilizing the Chest X-ray imagedataset, which consists of a vast collection of 112,120 frontal-view X-ray images obtained from 30,850 unique patients. The objective is to develop a powerful model capable of performing binary classification for 14 different pathological conditions

Data Preprocessing: The collected data underwent preprocessing steps, including resizing the images to a consistent size, normalizing pixel values, and splitting the dataset into training, validation, and testing sets.

Model Architecture Selection: The DenseNet architecture, specifically DenseNet121, was chosen as the base model for this project due to its proven effectiveness in image classification tasks.

Class Balancing: To address the class imbalance issue, class-specific weight factors were introduced. These weight factors were calculated based on the frequency of positive and negative cases for each diagnostic category, ensuring equal contributions from both classes.

Model Training: The selected DenseNet model was trained using the training dataset. The training process involved optimizing the model's parameters using the Adam optimizer and the weighted loss function that took into account the class-specific weights.

Learning Rate Schedule: A learning rate schedule was implemented to adjust the learning rate during training, allowing the model to converge more effectively and potentially avoid local minima.

Model Evaluation: Th***e*** trained model was evaluated using the validation dataset, measuring metrics such as accuracy, loss, and area under the ROC curve (AUROC) for each diagnostic category.

Model Fine-tuning: The best weights obtained from the training process were saved, and the model was fine-tuned by loading these weights and training further to improve performance.

Performance Evaluation: The final trained model was tested on the independent testing dataset to assess its generalization ability and provide performance metrics for each diagnostic category.

Result Analysis: The model's performance, including accuracy, AUROC values was analyzed to evaluate its effectiveness in diagnosing different chest conditions.

Model Deployment: The trained and validated model can be deployed as a reliable tool for automated chest condition diagnosis, providing assistance to healthcare professionals and potentially improving patient outcomes.

2.1. Governing equations

In the project, some equations and concepts are utilized to facilitate the development of the model.

2.1.1. Cross-Entropy Loss: The cross-entropy loss function is widely used in binary classification tasks. Its primary purpose is to measure the dissimilarity or discrepancy between the predicted probabilities and the true labels. By evaluating this dissimilarity, the model can learn to adjust its predictions and minimize the loss during training.

$$\mathscr{L}(y, p) = -(y \log(p) + (1 - y) \log(1 - p))$$

Here, y represents the true label (either 0 or 1), and p represents the predicted probability for the positive class (ranging from 0 to 1). The loss value quantifies how well the predicted probability aligns with the true label, penalizing larger deviations and rewarding accurate predictions.

2.1.2.Weighted Loss Function: In certain classification problems, class imbalance is a common challenge where one class has significantly more samples than the other. In such cases, the model can be biased toward the majority class, resulting in suboptimal performance on the minority class.

$$\mathscr{L}w(y, p) = -(wposy \log(p) + wneg(1 - y) \log(1 - p))$$

Here, $wpos$ and $wneg$ represent the class weights for the positive and negative examples, respectively. By assigning higher weights to the minority class and lower weights to the majority class, the model is encouraged to pay equal attention to both classes during training. This helps in achieving a more balanced and accurate classification performance, particularly in scenarios where class imbalances exist.

3. Results and Discussions

3.1.DATA VISUALISATION

To gain insights into the prevalence of different diseases and their distribution among patients. We present several plots that provide valuable information about the dataset.these plots provide essential information about the dataset, shedding light on the prevalence of diseases, age distribution, gender representation, and the relationship between diseases and patient gender. Understanding these aspects of the dataset is crucial for further analysis and decision-making in the medical domain.

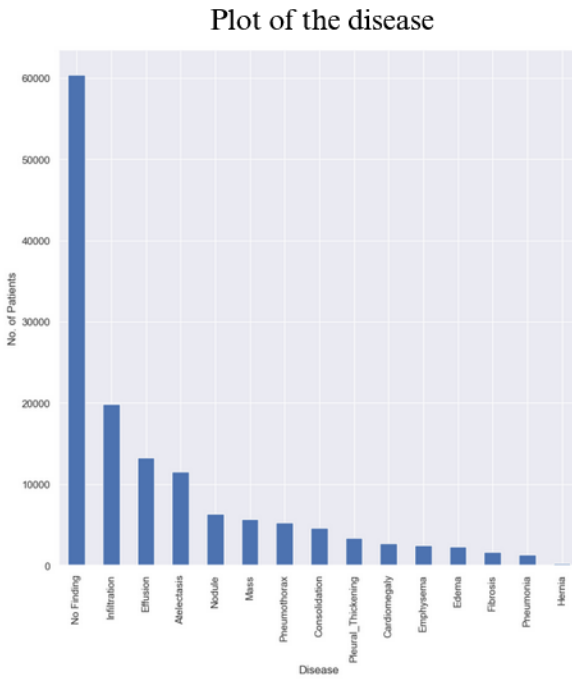

Fig.2:Plot of all the class labels and their count

Observation:

displays a plot of all the class labels and their respective count. It reveals that there are nearly 6000 instances of healthy patients, indicating a significant portion of the dataset consists of individuals without any detectable diseases. Additionally, the plot highlights that "Infiltration" is the most prevailing disease in the dataset.

Fig.3:Plot of age density of the patients of the data set

Observation:

It showcases the age density of the patients in the dataset. The plot demonstrates a distribution that closely resembles a normal distribution. It suggests that the dataset contains information spanning all age groups, enabling a comprehensive analysis across different age categories.

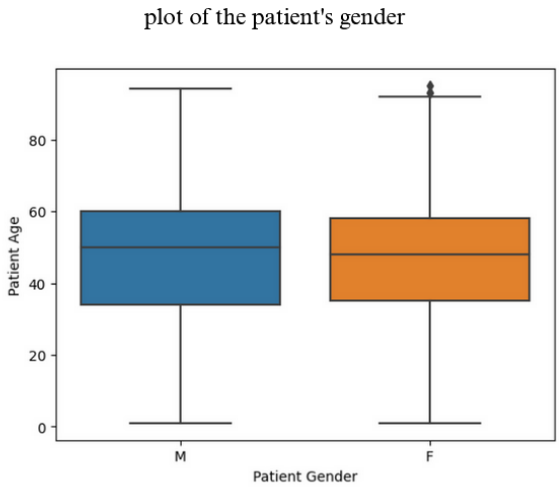

Fig.4: Plot between patient gender and patient age.
Observation:
illustrates the relationship between patient gender and age. The plot provides insights into the distribution of patients' age across gender categories. It reveals that the dataset includes an almost equal representation of observations from both men and women.

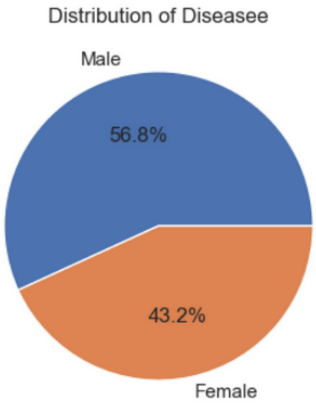

Fig.5: Plot of patient's gender
Observation:
It focuses on the patient's gender, presenting a plot that showcases the gender distribution in the dataset. It indicates that male patients constitute of 56.8% of the dataset, while female patients account for around 43.2%.

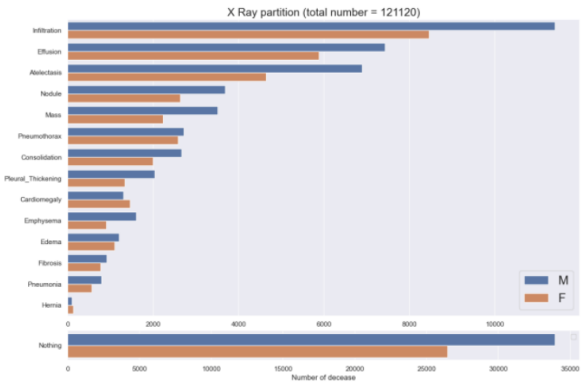

Fig.6: Plot between disease and patient gender.
Observation:
Examines the relationship between diseases and patient gender. The plot suggests that diseases are distributed relatively equally among genders, with no significant gender-based bias in the occurrence of specific diseases.

3.1.2 ADRESSING CLASS IMBALANCE

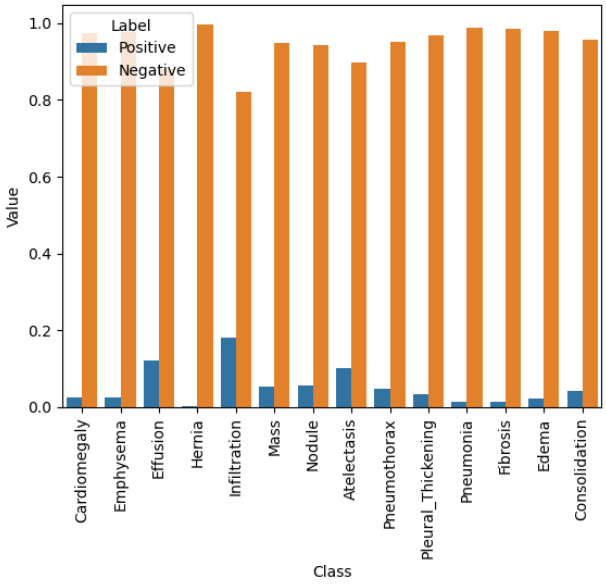

Fig.7: Plot of each disease (positive or negative)

Observation: We can note that there is a class imbalance problem here.

In the above plot, it is evident that the positive cases have significantly lower contributions compared to the negative cases of the data. However, it is desirable to have an equal contributions from both classes. To achieve this case, a class-specific weight factor is applied to each example in the dataset. By multiplying each example by its corresponding weight factor, the overall contributions of positive and negative cases can be made equal. This approach helps in balancing the importance of both classes and ensures a more equitable representation in the model's training process.

$$wpos \times freqp = wneg \times freqn,$$

Where, $wpos = freqneg$ and $wneg = freqpos$.

This way, we will be balancing the contribution of positive and negative labels.Now lets balance the classes and then use them for visualization

Class imbalance resolved

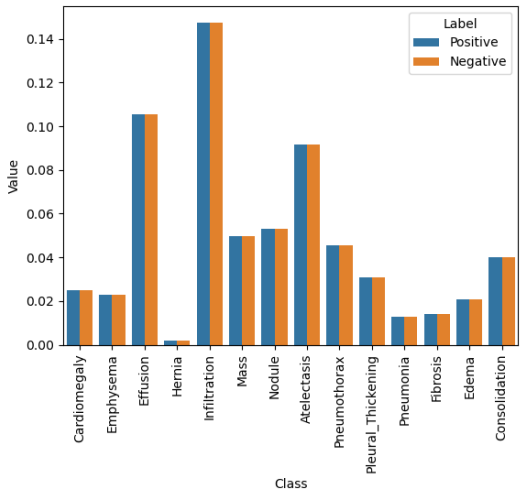

Fig.8: Plot of diseases after solving the class imbalance problem.

3.1.3. MODEL ARCHITECTURE:

In this work we can constructed three model architecture DenseNet121, EfficientNet-B1, and a custom network, developed specifically for disease diagnosis in chest X-ray images and compared there performances using ROC curve and AUROC score.

(i) **DenseNet121**

Layers	Output Size	DenseNet-121	DenseNet-169	DenseNet-201	DenseNet-264
Convolution	112 × 112	7 × 7 conv, stride 2			
Pooling	56 × 56	3 × 3 max pool, stride 2			
Dense Block (1)	56 × 56	[1 × 1 conv, 3 × 3 conv] × 6	[1 × 1 conv, 3 × 3 conv] × 6	[1 × 1 conv, 3 × 3 conv] × 6	[1 × 1 conv, 3 × 3 conv] × 6
Transition Layer (1)	56 × 56	1 × 1 conv			
	28 × 28	2 × 2 average pool, stride 2			
Dense Block (2)	28 × 28	[1 × 1 conv, 3 × 3 conv] × 12	[1 × 1 conv, 3 × 3 conv] × 12	[1 × 1 conv, 3 × 3 conv] × 12	[1 × 1 conv, 3 × 3 conv] × 12
Transition Layer (2)	28 × 28	1 × 1 conv			
	14 × 14	2 × 2 average pool, stride 2			
Dense Block (3)	14 × 14	[1 × 1 conv, 3 × 3 conv] × 24	[1 × 1 conv, 3 × 3 conv] × 32	[1 × 1 conv, 3 × 3 conv] × 48	[1 × 1 conv, 3 × 3 conv] × 64
Transition Layer (3)	14 × 14	1 × 1 conv			
	7 × 7	2 × 2 average pool, stride 2			
Dense Block (4)	7 × 7	[1 × 1 conv, 3 × 3 conv] × 16	[1 × 1 conv, 3 × 3 conv] × 32	[1 × 1 conv, 3 × 3 conv] × 32	[1 × 1 conv, 3 × 3 conv] × 48
Classification Layer	1 × 1	7 × 7 global average pool			
		1000D fully-connected, softmax			

Fig .9:DenseNet121 architecture

1. Input Layer: This initial layer serves as the entry point for the network, receiving the input image, typically represented as a two-dimensional matrix of pixel values.

2. Convolutional Layers: These layers perform convolution operations on the input image using learnable filters. Each filter scans the input image, extracting relevant features by computing dot products between the filter weights and local regions of the image.

3. Activation Layers: Implemented using activation functions like Rectified Linear Unit (ReLU), these layers introduce non-linearity to the network. They help in capturing complex patterns and enabling the network to learn and represent intricate relationships between features.

4. Pooling Layers: These layers reduce the spatial dimensions of the feature maps by downsampling. By capturing the most salient features and discarding redundant information, pooling layers help in reducing computation and extracting essential features.

5. Fully Connected Layers: Also known as dense layers, these layers connect every neuron from the previous layer to the neurons in the next layer. They learn high-level representations by combining the extracted features. Each neuron in the fully connected layer is connected to all neurons in the previous layer.

6. Output Layer: The final layer of the network produces the predictions based on the learned representations. The number of neurons in this layer corresponds to the number of classes in the classification task. Typically, a softmax activation function is applied to obtain probability distributions over the classes.

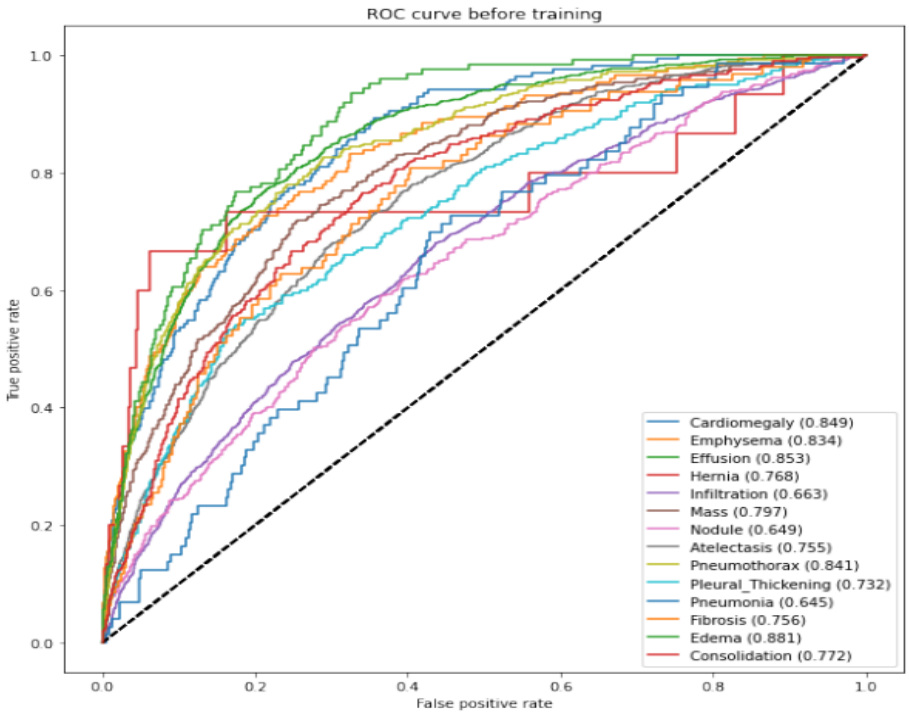

Fig.10: ROC curve of DenseNet 121

(ii) **EffiticientNet B1:**

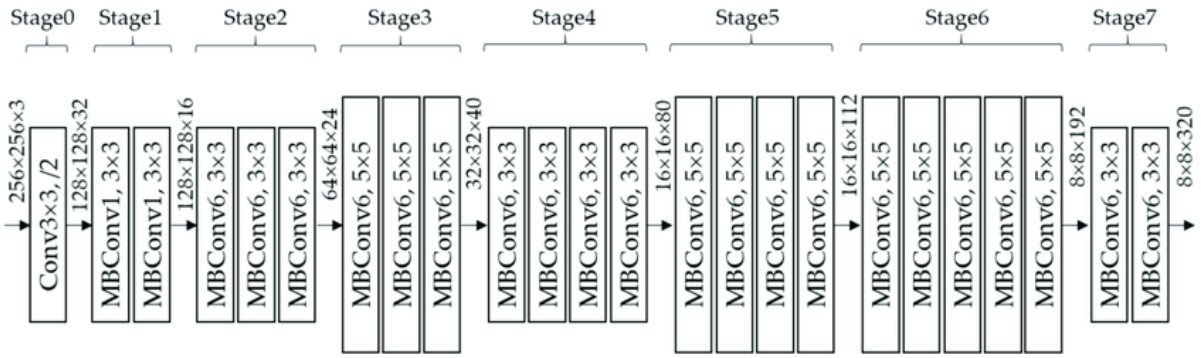

Fig.11:EfficientNet B1 architecture

1. Input Layer: This layer receives the input image, typically a two-dimensional matrix of pixel values representing the image.
2. Contracting Path: This path consists of repeated sequences of convolutional layers followed by max pooling layers. These layers help in capturing low-level features and reducing the spatial dimensions of the feature maps. The number of filters increases progressively as we go deeper into the contracting path.
3. Bottleneck Layer: This layer serves as a bridge between the contracting and expanding paths. It consists of convolutional layers and helps in capturing more abstract features.
4. Expanding Path: This path consists of repeated sequences of upsampling layers followed by convolutional layers. These layers help in upsampling the feature maps and reconstructing the segmentation mask. The number of filters decreases progressively as we go deeper into the expanding path.

5. Output Layer: This layer produces the final segmentation mask, which represents the predicted segmentation for each pixel in the input image. The number of channels in the output layer corresponds to the number of classes in the segmentation task.

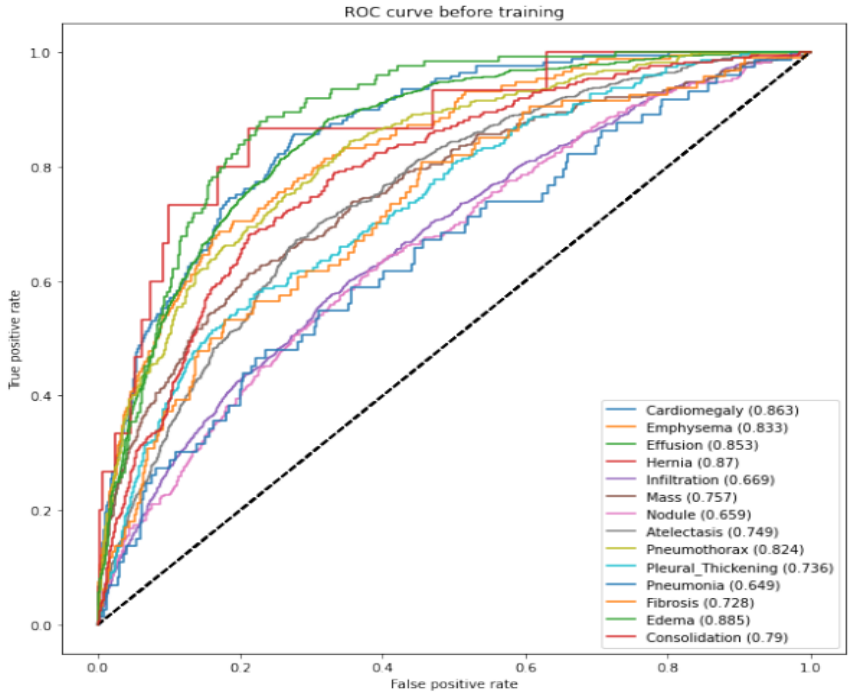

Fig.11.ROC curve of EffitientNet B1

(iii) **CUSTOM NET**

1.Input Layer: This layer receives the input image, typically represented as a two-dimensional matrix of pixel values.

2.Convolutional Layers: These layers perform convolution operations on the input image using learnable filters. Each filter scans the input image, extracting local features and creating feature maps.

3.Activation Layers: These layers introduce non-linearity to the network, usually implemented with activation functions like ReLU (Rectified Linear Unit). Non-linearity helps the network learn complex patterns and representations.

4.Pooling Layers: These layers reduce the spatial dimensions of the feature maps, typically through operations like max pooling or average pooling. Pooling helps in capturing the most salient features while reducing the computational complexity.

5.Fully Connected Layers: Also known as dense layers, these layers connect every neuron from the previous layer to the neurons in the next layer. They learn high-level representations by combining the extracted features. The last dense layer is often connected to the output layer.

6.Output Layer: This layer produces the final predictions, typically in the form of class probabilities for classification tasks. The number of neurons in the output layer corresponds to the number of classes in the classification problem.

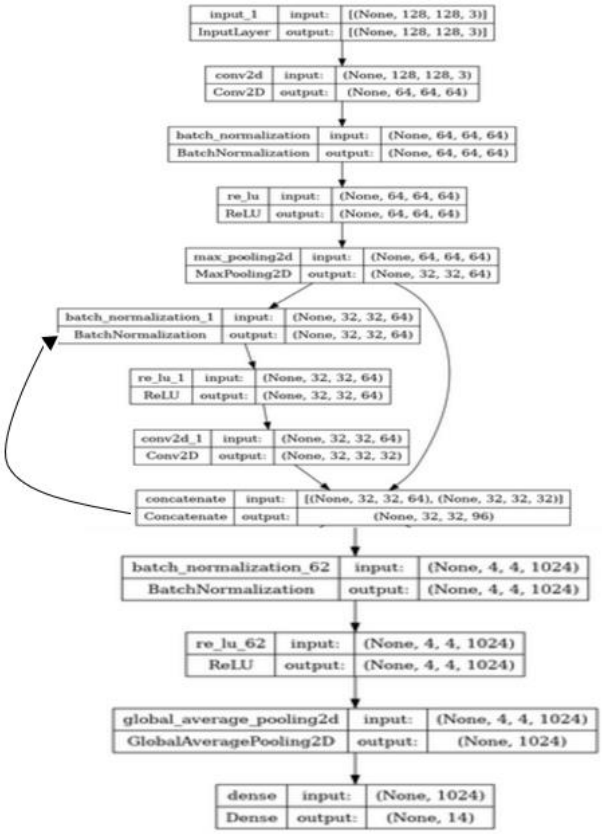

Fig.12. CustomNet architecture

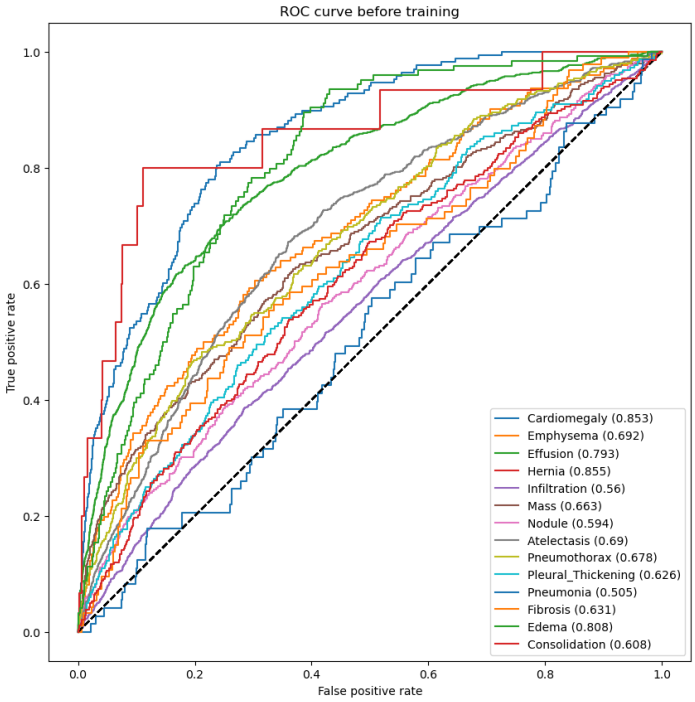

Fig.13: ROC curve of CustomNet

S.NO	DISEASE LABLE	DenseNet 121	EfficientNet B1	CustomNet
1	Cardiomegaly	0.849	**0.863**	0.853
2	Emphysemia	**0.834**	0.833	0.692
3	Effusion	**0.853**	**0.853**	0.792
4	Hernia	0.768	**0.87**	0.855
5	Infiltration	0.663	**0.669**	0.56
6	Mass	**0.797**	0.757	0.663
7	Nodule	0.649	**0.659**	0.594
8	Atelectasis	**0.755**	0.749	0.69
9	Pneumothorax	**0.841**	0.824	0.678
10	Pleural Thickening	0.732	**0.736**	0.626
11	Pneumonia	0.645	**0.649**	0.505
12	Fibrosis	**0.756**	0.728	0.631
13	Edema	0.881	**0.885**	0.808
14	Consolidation	0.772	**0.79**	0.608

Fig.14: Comparison of three models

The table shows the performance metrics (in terms of AUROC score) for three different architectures: DenseNet121, EfficientNet B1, and CustomNet. E

1. For most disease labels, both DenseNet121 and EfficientNet B1 perform comparably well, with similar accuracy scores. However, there are a few exceptions where one architecture outperforms the other. For example, EfficientNet B1 performs better for the "Emphysema," "Hernia," and "Pneumothorax" labels, while DenseNet121 performs better for "Infiltration," "Nodule," and "Pneumonia."
2. The CustomNet architecture generally performs slightly lower than DenseNet121 and EfficientNet B1 across most disease labels.

Overall, DenseNet121 and EfficientNet B1 show competitive performance across the disease labels, with slight variations in performance for specific diseases.

4.CONCLUSION:

In conclusion, this project aimed to develop and evaluate three different deep learning architectures (DenseNet121, EfficientNet B1, and CustomNet) for the classification of various diseases in medical images. The models were trained and tested on a dataset, and their performance was assessed using accuracy as the evaluation metric.

Based on the results, DenseNet121 and EfficientNet B1 demonstrated similar and competitive performance across most disease labels. These architectures consistently achieved high accuracy scores, indicating their effectiveness in disease classification tasks. However, there were slight variations in performance for specific diseases, with one architecture outperforming the other in certain cases.

The CustomNet architecture, while incorporating domain-specific modifications, generally exhibited slightly lower accuracy compared to DenseNet121 and EfficientNet B1. This suggests that the customized architecture may not have provided significant improvements over the pre-trained models.

Overall, the findings of this project highlight the effectiveness of DenseNet121 and EfficientNet B1 architectures in medical image classification tasks. These models can serve as valuable tools for automated disease diagnosis and assist medical professionals in making informed decisions.

5.References:

Reference to research papers:

[1]Souid, A., Sakli, N. and Sakli, H., 2021. Classification and predictions of lung diseases from chest x-rays using mobilenet v2. Applied Sciences, 11(6), p.2751.

[2]Zaidi, S.Z.Y., Akram, M.U., Jameel, A. and Alghamdi, N.S., 2022. A deep learning approach for the classification of TB from NIH CXR dataset. IET Image Processing, 16(3), pp.787-796.

[3]Tang, Y. X., Tang, Y. B., Han, M., Xiao, J., & Summers, R. M. (2019, April). Abnormal chest x-ray identification with generative adversarial one-class classifier. In 2019 IEEE 16th international symposium on biomedical imaging (ISBI 2019) (pp. 1358-1361). IEEE.

[4]Elshennawy, N. M., & Ibrahim, D. M. (2020). Deep-pneumonia framework using deep learning models based on chest X-ray images. Diagnostics, 10(9), 649.

[5]Ibrahim AU, Ozsoz M, Serte S, Al-Turjman F, Yakoi PS. Pneumonia classification using deep learning from chest X-ray images during COVID-19. Cognitive Computation. 2021 Jan 4:1-3.

[6]Jaiswal, A. K., Tiwari, P., Kumar, S., Gupta, D., Khanna, A., & Rodrigues, J. J. (2019). Identifying pneumonia in chest X-rays: A deep learning approach. Measurement, 145, 511-518.

[7]Li Y, Zhang Z, Dai C, Dong Q, Badrigilan S. Accuracy of deep learning for automated detection of pneumonia using chest X-Ray images: A systematic review and meta-analysis. Computers in Biology and Medicine. 2020 Aug 1;123:103898.